Available online at www.sciencedirect.com

ScienceDirect

Scripta Materialia 72–73 (2014) 5–8

Scripta MATERIALIA

www.elsevier.com/locate/scriptamat

A novel, single phase, non-equiatomic FeMnNiCoCr high-entropy alloy with exceptional phase stability and tensile ductility

M.J. Yao, K.G. Pradeep,** C.C. Tasan* and D. Raabe

Max-Planck-Institut für Eisenforschung GmbH, Max-Planck-Str. 1, 40237 Düsseldorf, Germany

Received 2 September 2013; accepted 29 September 2013
Available online 5 October 2013

A non-equiatomic FeMnNiCoCr alloy is introduced and characterized at multiple scales employing various characterization techniques (e.g. atom probe tomography, electron channeling contrast imaging, electron backscatter diffraction, etc.) to elucidate (i) the role of configurational entropy and (ii) the intrinsic tensile ductility of high-entropy alloys. Results reveal that the new material is a true high-entropy alloy with a stable random solid solution despite its comparably low configurational entropy, and that it has excellent tensile ductility irrespective of the substantial lattice distortion.

Keywords: Non-equiatomic; High-entropy alloy; Atom probe tomography; Ductility; ECCI

High-entropy alloys (HEAs) are multi-component systems based on the novel alloy design strategy of configurational entropy (CE) maximization. This strategy aims at a reduction of Gibbs free energy by the increase in CE [1], to design phases with simple structures, rather than brittle ordered intermetallics typical of many multi-component systems [2–4]. As a result of multiple alloy components creating strong lattice distortion, HEAs are promising candidates for many potential applications with expectedly high solid-solution strengthening and excellent resistance to high-temperature softening [2,3,5].

To this end, HEAs were initially defined to consist of at least five principal elements of concentrations between 5 and 35 at.%, in order to maximize the CE and facilitate the formation of solid solutions. Recent reports, however, have questioned such a dominant role of the CE independent of the mixing enthalpy, and have stressed that the Gibbs free energy is decisive for phase formation, even in cases of increased CE [6,7]. While the role of the CE is still under debate, it is interesting to note that the majority of the introduced HEAs still follow the original concentration design criterion, i.e. near-equiatomic ratios, while non-equiatomic HEAs have rarely been investigated.

On the other hand, although many HEAs have been designed and studied recently, their tensile test performance was rarely documented [8–13]. Instead, mechanical properties were often characterized in terms of compression tests or hardness. In fact, with the exception of a very recent work reporting good ductility [13], most of the HEAs designed to date have very limited tensile ductility, often not exceeding a few percent of strain prior to fracture. In this context it appears essential to better understand whether the limited ductility is arising from processing issues (e.g. due to consolidation problems during mechanical alloying), characterization issues (e.g. due to undetected intermetallic phase formation[1]) or due to any unknown intrinsic limitations of such multi-component systems with strong solid-solution hardening.

This study aims at improving our understanding on these points, namely: (i) the role of CE in the phase formation, and (ii) the true tensile behavior of HEAs. For this purpose we introduce a novel $Fe_{40}Mn_{27}Ni_{26}Co_5Cr_2$ (at.%) HEA, which offers several advantages in the context mentioned above: its CE (i.e. 10.8 J K^{-1} mol^{-1}, equal to ~130% of gas constant, R) is higher than the fusion entropy of most metals (i.e. ~R), and hence fits well into the HEA definition. Its CE is, however, ~20% lower compared to that of a recently suggested equiatomic FeMnNiCoCr HEA [4,7,13]. This difference enables us to study the role of the entropy component on the stability and tensile

* Corresponding author. Tel.: +49 2116792866; e-mail addresses: c.tasan@mpie.de, c.tasan@tue.nl

** Corresponding author. Tel.: +49 211 6792 336; e-mail address: kg.prad@mpie.de

[1] X-ray diffraction, the standard technique employed in HEA characterization, is not fully reliable in detecting sub-micron intermetallic phases [6,19], requiring atom probe tomography measurements for full structural analysis.

1359-6462/$ - see front matter
http://dx.doi.org/10.1016/j.scriptamat.2013.09.030

behavior of HEAs. Also, the effects of consolidation issues or brittle intermetallic phases are ruled out through liquid-metallurgical processing and characterization down to the atomic scale, allowing assessment of the intrinsic tensile ductility of the designed material.

The alloy was melted from pure metals (purity > 99.8 wt.%) in a vacuum induction furnace, cast into a water-cooled copper mold and furnace-cooled. Following hot-rolling to 50% thickness reduction at 900 °C, it was homogenized at 1200 °C for 2 h in Ar atmosphere, and quenched in water. Further grain refinement was achieved through cold-rolling to 64% thickness reduction and subsequent 900 °C annealing in Ar atmosphere for 10 min.

The characterization of phase formation and thermal stability was carried out by X-ray diffraction (XRD) and differential scanning calorimetry (DSC), respectively. During XRD, specimens were mounted on a Huber-2 goniometer and exposed to Co K_α radiation ($\lambda = 1.79$ Å). The Metero0D detector swept a 2θ range from 0° to 120° with a step size of $\Delta 2\theta = 0.05°$. DSC experiments were performed in a SETARAM Setsys 16/18 device between 20 °C and 1300 °C at different rates (5–10 K min^{-1}) in Ar atmosphere.

Microstructure characterization was carried out on as-cast, hot-rolled, homogenized, cold-rolled and recrystallized samples. Here we focus on the homogenized state. Secondary electron (SE) imaging, energy-dispersive X-ray spectroscopy (EDX) and electron backscatter diffraction (EBSD) were conducted in a 6500F JEOL field emission gun-scanning electron microscope (FEG-SEM) equipped with an EDAX software and a TSL OIM EBSD system. Elemental distribution at atomic scale was studied using a local electrode atom probe tomography (APT) (LEAP 3000X HR, Cameca Inc.). Tip specimens for APT were prepared in a FEI Helios Nanolab 600i dual-beam focused ion beam (FIB) device as described in Ref. [14]. To verify the chemical homogeneity in the vicinity of grain boundaries (most favorable positions for intermetallics [6]), two tips were lifted out from areas adjacent to a grain boundary, one from a (<001>//ND) oriented grain and the other from a (<111>//ND) oriented grain.

Mechanical properties of homogenized, cold-rolled and recrystallized states were evaluated at room temperature, with a strain rate of 2.5×10^{-3} s^{-1} using a Kammrath & Weiss stage and dog-bone-shaped specimens of gauge geometry of 4 mm × 2 mm × 1 mm. For trace analysis, samples with a gauge geometry of 10 mm × 7 mm × 1 mm were deformed to 3%, 13% and 28% strain. Prior to tensile deformation, one surface of these samples was polished for trace analysis, while a speckle pattern was applied to the other surface for digital image correlation analysis (Aramis, GOM GmbH) [15,16].

To reveal the deformation mechanisms, microstructures of homogenized samples were investigated after the tests using multi-focus imaging with a Leica DM 4000M optical microscope (OM) for trace analysis, and quantitative electron channeling contrast imaging (ECCI) [17] in a FEG/FIB dual-beam Zeiss-crossbeam XB1560 FIB-SEM, for the evolution of the dislocation structures.

First, XRD and DSC results of the as-cast and homogenized states are presented (Fig. 1). Both XRD patterns show only single-phase face-centered cubic (fcc) peaks (lattice parameter = 3.60 Å), indicating a single-phase

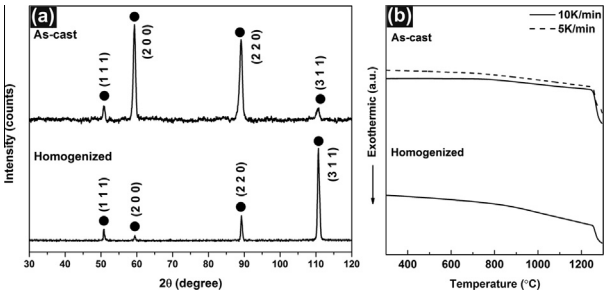

Figure 1. (a) XRD patterns and (b) DSC heating curves of as-cast and homogenized states.

solid solution in both states. DSC heating curves obtained at a low heating rate of 5 K min^{-1} reveal no exothermic or endothermic phase transformation peaks up to melting point (~1250 °C). These data show that the material consists of a very stable fcc phase.

Figure 2a and b shows the homogenized alloy in fully recrystallized state with equiaxed grains containing annealing twins. The EBSD scan at the same area (1 μm step size) (Fig. 2c) and high-resolution EBSD measurements (100 nm step size) (Fig. 2d) confirm the presence of a single fcc phase. Unindexed points arise from 0.6 vol.% porosity.

For mapping the compositional homogeneity, EDX maps of the same area in Figure 2b and c are presented (Fig. 2e). All elements are homogeneously distributed, except for some minor inhomogeneity due to the formation of manganese oxides, which is a typical processing effect in high Mn alloys [7,12]. For studying chemical homogeneity at atomic scale, APT measurements were carried out: no segregation or enrichment was observed in the analyzed volumes of 98 × 97 × 117 nm^3 and 90 × 90 × 141 nm^3 of representative concentrations $Fe_{40.3}Mn_{26.0}Ni_{25.6}Co_{6.1}Cr_{2.0}$ and $Fe_{40.8}Mn_{27.1}Ni_{24.1}Co_{5.7}Cr_{2.3}$ (Fig. 2f and g), respectively. One-dimensional concentration–depth profiles of all elements are plotted along a cylindrical region of interest with a diameter of 10 nm through the analyzed volume, revealing no statistically significant concentration fluctuations (Fig. 2f_2 and g_2). The statistics of the elemental distribution are further quantified by a binomial analysis. The frequency distribution of the elemental concentrations in both analyzed volume portions matches the reference binomial random distributions very well (Fig. 2f_3 and g_3). The relative deviation from randomness is evaluated in terms of several parameters, as listed in the inset table. μ, as a normalized auto-correlation parameter of χ^2, can assume values between 0 and 1, where 0 represents randomness and 1 represents complete association with solutes of the same type [18]. In the two analyzed tips, all elements show μ values close to 0, i.e. practically complete randomness. All these analyses give proof of a random single fcc solid solution, confirmed down to atomic scale.

These results enable us to come back to the first discussion point mentioned above, namely to the role of CE on phase formation in multi-component alloys. Despite its significantly lower CE compared to the equiatomic FeMnNiCoCr system [7], the introduced non-equiatomic HEA consists of a very stable single phase solution up to the melting point. This result supports previous work, where the formation of multiple phases

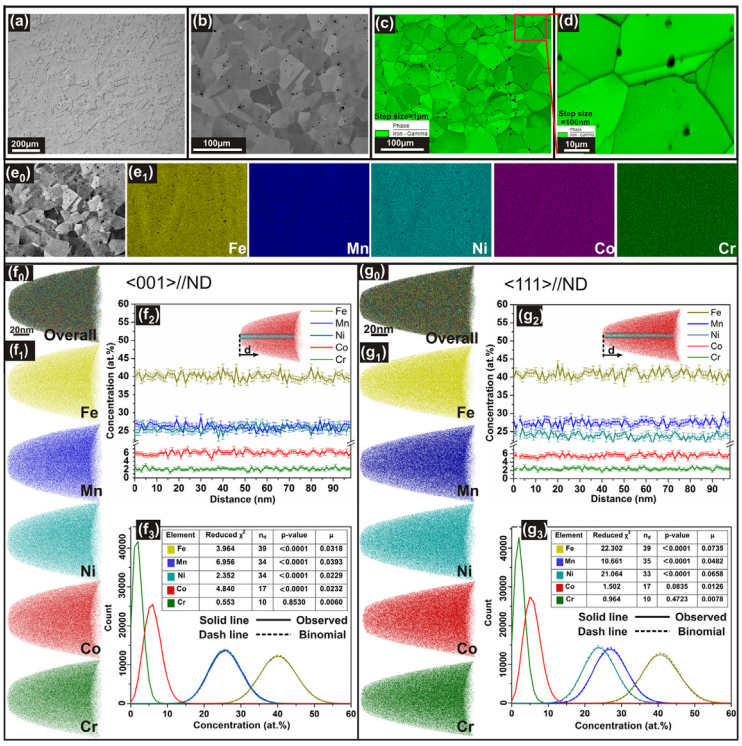

Figure 2. Homogenized microstructure: (a) OM image; (b) SE image; (c, d) low- and high-resolution EBSD phase maps with image quality overlay; (e) EDX maps of the same area; (f, g) element distribution analyses from two APT tips. The three-dimensional elemental maps, individual elemental distributions, concentration–depth profiles of all elements (bin size of 1 nm) and binomial distribution of analyzed data in comparison to the theoretical binomial random distribution are provided respectively from (0) to (3).

in equiatomic HEAs with high CE were reported [6,19], on the relatively indecisive role of maximizing the CE as an essential criterion for the overall phase formation in HEAs. It can, therefore, be concluded, considering the composition and constitution of the alloy presented here, that the original design criterion on component composition of 5–35 at.% is not a fully sufficient (or necessary) requirement for achieving single phase solutions in multi-component systems.

Figure 3 shows the mechanical behavior of the new HEA in a homogenized state, exhibiting a yield strength (YS) of ~95 MPa, an ultimate tensile strength (UTS) of ~375 MPa and a total elongation (TE) of ~58%. Despite its low YS, the alloy possesses an excellent strain-hardening capability and thus very high ductility. This excellent mechanical response is attributed to the presence of a single fcc phase microstructure that is free of any intermetallics or ordered phases.

Cold-rolling increases UTS to ~760 MPa but reduces ductility to ~17%. The EBSD map of the cold-rolled state before the tensile test shows a microstructure consisting of 99% fcc phase with low pattern quality near grain boundaries, likely due to high dislocation densities (Fig. 3a). No phase transformation is observed, either before or after the tensile test, confirming the stability of the fcc phase, also when subjected to heavy plastic deformation. The increase in UTS is attributed to massive dislocation–dislocation interactions, while the ductility deteriorates due to the gradual loss in compensating strain localization by retained strain hardening [20].

Follow-up annealing at 900 °C for 10 min produces an average grain size of ~12 μm, i.e. ~50% of the

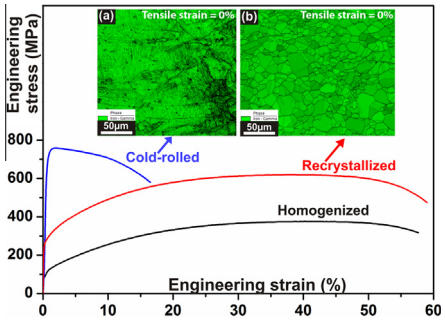

Figure 3. Stress–strain curves of different states. Inset shows EBSD phase and IQ maps of undeformed (a) cold-rolled and (b) recrystallized samples.

homogenized state (Fig. 3b). The YS and UTS are significantly enhanced by grain refinement (~150% to ~240 MPa, and ~72% to ~645 MPa, respectively) with no reduction in ductility. This unexpectedly strong Hall–Petch effect suggests not only an efficient reduction in the mean free dislocation path but also a surprisingly high grain boundary resistance against slip transfer. In essence, this strong Hall–Petch effect requires higher external stresses to enable co-deformation of neighboring grains and hence strain compatibility.

Some of the underlying deformation mechanisms can be discussed based on the surface and cross-section analyses in Figure 4. At 3% strain, the sample surface exhibits distinct slip lines, oriented differently inside grains of different orientation but parallel within each grain (Fig. 4a$_1$). In some grains, two groups of slip lines of different inclination can be distinguished. At larger strains (13%) more groups of slip lines are present inside

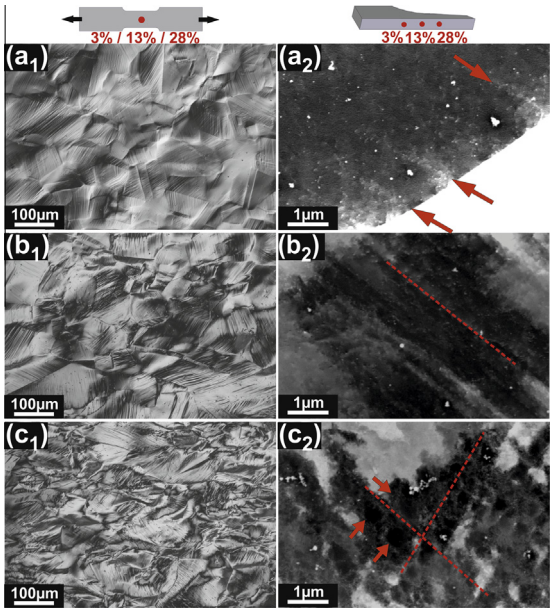

Figure 4. Deformation microstructure revealed by (1) OM and (2) ECCI, at strain levels of (a) 3%, (b) 13%, (c) 28%.

most grains. At 28% deformation we observe strong plastic distortions of the grains (Fig. 4c_1). The surface trace analysis strongly suggests dislocation-plasticity and associated crystallographic microbanding as mesoscopic deformation mechanisms in this material. EBSD-based trace analysis (not shown here) reveals that the traces are dominantly in {1 1 1} planes.

The grain substructure was investigated in more detail by ECCI. At 3% strain, in the vicinity of GBs, dislocations (appearing white in the otherwise dark grain), are piled up along certain planes (see arrows in Fig. 4a_2). At 13%, a planar dislocation substructure is developed, indicating the presence of planar slip (Fig. 4b_2). Such substructures have characteristic highly dense dislocation walls (HDDWs, see dashed lines), formed by the arrangement of dislocations in planar arrays [21], with low dislocation density zones in between. At 28% strain dislocation cell structures (see arrows in Fig. 4c_2) are formed in the initially dislocation depleted areas in between the HDDWs, suggesting the activation of wavy slip.

These results confirm that the introduced alloy is dominantly deformed by dislocation slip and not by twinning. Planar slip is promoted by short range ordering, increase of the friction stress or reduction of stacking fault energy (SFE) [21]. For a random solid solution the contribution of the former cannot be significant. Considering the absence of deformation twinning, the SFE of this alloy is relatively moderate, suggesting that the contribution of the latter is also insignificant. Therefore, the dominant mechanism promoting the incipient planar slip is the strong friction stress on dislocation motion, arising from the solutal lattice distortion. For higher strain levels above ~20%, more slip planes are activated and the density of dislocations significantly increases, both of which rendering dislocation cross-slip more frequent, resulting in dislocation clustering and cell formation. Such ongoing generation and activation mechanisms of dislocation slip also at higher strains explains the high strain hardening capacity and hence ductility of this HEA.

These results clearly show that limited room temperature tensile ductility is not an intrinsic property of HEA, highlighting that multi-component alloy systems can be considered for a wider range of applications demanding high ductility and strength.

In summary, a novel, single phase, non-equiatomic $Fe_{40}Mn_{27}Ni_{26}Co_5Cr_2$ (at.%) HEA is introduced, revealing novel design principles in terms of the role of CE and intrinsic tensile ductility. The microstructure of this cast HEA is fully characterized down to atomic resolution, revealing a random single-phase solid solution. The achievement of a random solution despite low CE underlines that equimolarity is not a fully necessary requirement for achieving single-phase solid solutions in multi-component systems. Moreover, being synthesized without porosity and brittle intermetallic phases, this alloy exhibits excellent tensile ductility (~60%), emphasizing that limited tensile ductility is not an intrinsic limitation of HEAs.

The authors would like to thank Dr Hauke Springer and Dr Pyuck-Pa Choi for their contributions.

[1] J.W. Yeh, S.K. Chen, S.J. Lin, et al., Adv. Eng. Mater. 6 (2004) 299–303.
[2] S. Varalakshmi, M. Kamaraj, B.S. Murty, Mater. Sci. Eng. A 527 (2010) 1027–1030.
[3] O.N. Senkov, G.B. Wilks, J.M. Scott, et al., Intermetallics 19 (2011) 698–706.
[4] B. Cantor, I.T.H. Chang, P. Knight, et al., Mater. Sci. Eng. A 375 (2004) 213–218.
[5] C.W. Tsai, Y.L. Chen, M.H. Tsai, et al., J. Alloy. Compd. 486 (2009) 427–435.
[6] K.G. Pradeep, N. Wanderka, P. Choi, et al., Acta Mater. 61 (2013) 4696–4706.
[7] F. Otto, Y. Yang, H. Bei, et al., Acta Mater. 61 (2013) 2628–2638.
[8] F.J. Wang, Y. Zhang, G.L. Chen, et al., Int. J. Mod. Phys. B 23 (2009) 1254–1259.
[9] T.T. Shun, Y.C. Du, J. Alloy. Compd. 479 (2009) 157–160.
[10] L. Liu, J.B. Zhu, C. Zhang, et al., Mater. Sci. Eng. A 548 (2012) 64–68.
[11] A.V. Kuznetsov, D.G. Shaysultanov, N.D. Stepanov, et al., Mater. Sci. Eng. A 533 (2012) 107–118.
[12] A. Gali, E.P. George, Intermetallics 39 (2013) 74–78.
[13] F. Otto, A. Dlouhý, C. Somsen, et al., Acta Mater. 61 (2013) 5743–5755.
[14] K. Thompson, D. Lawrence, D.J. Larson, et al., Ultramicroscopy 107 (2007) 131–139.
[15] D. Raabe, M. Sachtleber, Z. Zhao, et al., Acta Mater. 49 (2001) 3433–3441.
[16] I. Gutierrez-Urrutia, S. Zaefferer, D. Raabe, Mater. Sci. Eng. A 527 (2010) 3552–3560.
[17] I. Gutierrez-Urrutia, S. Zaefferer, D. Raabe, Scripta Mater. 61 (2009) 737–740.
[18] M.P. Moody, L.T. Stephenson, A.V. Ceguerra, et al., Microsc. Res. Tech. 71 (2008) 542–550.
[19] S. Singh, N. Wanderka, B.S. Murty, et al., Acta Mater. 59 (2011) 182–190.
[20] I. Gutierrez-Urrutia, D. Raabe, Acta Mater. 60 (2012) 5791–5802.
[21] I. Gutierrez-Urrutia, D. Raabe, Acta Mater. 59 (2011) 6449–6462.